Growth Mechanism Deconvolution of Self-Limiting Supraparticles Based on Microfluidic System

Qiang Fu,[†,‡] Yuping Sheng,[§] Hongjie Tang,[⊥] Zhening Zhu,[⊥] Mingbo Ruan,[†] Weilin Xu,[*,†] Yutian Zhu,[*,§] and Zhiyong Tang[*,⊥]

[†]State Key Laboratory of Electroanalytical Chemistry, Jilin Province Key Laboratory of Low Carbon Chemical Power, Changchun Institute of Applied Chemistry, Chinese Academy of Science, 5625 Renmin Street, Changchun 130022, P.R. China, [‡]Graduate University of Chinese Academy of Science, Beijing 100049, China, [§]State Key Laboratory of Polymer Physics and Chemistry, Changchun Institute of Applied Chemistry, Chinese Academy of Sciences, Changchun 130022, P.R. China, and [⊥]National Center for Nanoscience and Technology, 11 Beiyitiao, Zhongguancun, Beijing, 100190, China

ABSTRACT The synthesis of colloidal supraparticles (SPs) based on self-assembly of nanoscopic objects has attracted much attention in recent years. Here, we demonstrate the formation of self-limiting monodisperse gold SPs with core–shell morphology based on the building blocks of flexible nanoarms in one step. A flow-based microfluidic chip is utilized to slow down the assembly process of the intermediates, which surprisingly allows for observation of ultrathin gold nanoplates as first intermediates. Notably, these intermediate cannot be observed in traditional synthesis due to their rapid rolling-up to form the second-order nanostructure of flexible hollow nanoarms. The growth mechanism of SPs can then be deconvoluted into two seed-mediated steps. Monte Carlo simulations confirm that the self-limiting growth of binary SPs is governed by a balance between electrostatic repulsion and van der Waals attraction.

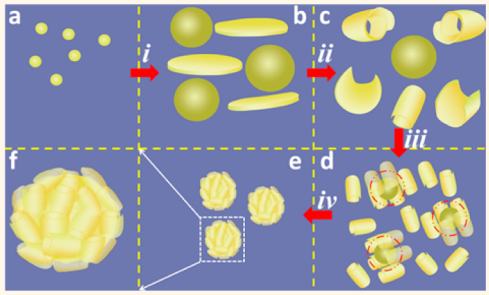

KEYWORDS: supraparticle · Au · growth mechanism · microfluidics · Monte Carlo simulation

Colloidal supraparticles (SPs) refer to nanoparticle assemblies in the form of colloidal particles.[1−3] The assembly of nanoparticles (1−100 nm in diameter) into higher-order nanostructures such as supercrystals and superlattice membranes provides a unique opportunity to produce materials with new collective physical, chemical, and mechanical properties,[4,5] which directly impact advances in solar cells, light-emitting diodes, and solid-state catalysts.[6,7] To date, several approaches have been developed for synthesizing colloidal SPs from constituent nanoparticles with uniform or nonuniform size distributions.[1,8−11] In these approaches, the building blocks of SPs must be prepared beforehand at high purity before self-assembly into SPs can occur at rigorous condition. Numerical simulations or theoretical calculations have been performed to elucidate the SP self-assembly process in greater detail,[2,11,12] but the intermediate structures, key to inferring growth mechanism, possess short lifetimes and as of yet have not been observed in traditional low-time-resolved synthetic approaches.

We present here a simple seed-mediated synthesis of self-limiting monodisperse gold SPs. In this method, the "one pot" synthesis of building blocks and the subsequent self-assembly occur in step over several minutes. The detailed seed-mediated growth mechanisms of both the building-blocks and the gold SPs are deconvoluted solidly by directing the reaction through a simple microfluidic system. This flow-based platform allows us to slow down the growth process of SPs, capture the "short-lifetime" intermediate subunits, then deduce their shape evolution mechanism. The intermediate subunits are the building blocks for the assembly of nanosized SPs, and usually cannot be discerned or obtained solely in the traditional synthesis process due to the rapid self-assembly of them for the growth of SPs.[11] The combination of microfluidics with traditional synthesis presented here represents a new powerful tool for understanding the intrinsic growth mechanism of

* Address correspondence to weilinxu@ciac.ac.cn, ytzhu@ciac.ac.cn, zytang@nanoctr.cn.

Received for review May 22, 2014 and accepted December 17, 2014.

Published online December 17, 2014
10.1021/nn5027998

varying nanomaterials. By slowing down the rapid assembly process, one can obtain the deeper and more precise information about previously unresolvable transient steps.

RESULTS AND DISCUSSION

The uniform nanosized gold SPs were synthesized by adopting a seed-mediated synthesis protocol at room temperature (for details see Supporting Information). In brief, the small gold seeds were synthesized first,[13] and then the seeds, growth solution with gold precursor and reductant were mixed together with gentle shaking until the solution color turned light blue (~20 s). The solution was left undisturbed for a time (typically under 10 min) to allow for particle growth. Figure 1a represents the typical TEM image of the obtained gold seeds with the average diameter of about 4 nm. On the basis of these seeds, spherical "meatball"-like nanoparticles rather than rounded nanoplates (59 ± 5 nm in diameter) (Figure 1b, Supporting Information Figure S1) were obtained. Similar methods have been extensively used to synthesize Au nanocubes or nanoplates by other groups, so the "meatball"-like shape is unexpected.[13−15] As an additional surprise, the high magnification TEM image shown in Figure 1c reveals each "meatball" to be comprised of many smaller subunits as opposed to as a single entity.[15,16] The high resolution TEM (HRTEM) images of a single "meatball"-like SP obtained here (Figure 1d,e, Supporting Information Figure S2) further indicate that the "meatball"-like SP is composed of flexible nanoarms splayed in a seemingly random fashion. This observation reveals that the "meatball"-like nanoparticles obtained here are SPs. The observed lattice fringes on individual nanoarm shown in Figure 1e correspond to the (111) facets of gold both because the *d*-spacing is 0.236 nm and the dihedral angle is around 60°, indicating that the nanoarm is single-crystalline. To the best of our knowledge, this is the first example of SPs synthesized in such a simple and rapid way.[2,11] Surface-rough "meatball"-like Au or Pt nanoparticles have been broadly reported before,[16−25] but all these individual "meatball"-like nanoparticles are single units rather than SPs. The X-ray diffraction (XRD) pattern of the SPs shows that the peaks can be indexed to a face-centered cubic unit cell (Figure 1f), in which 2θ values of 39.75°, 46.23°, 67.45°, and 81.24° can be indexed to diffraction of the (111), (200), (220), and (311) planes of gold, respectively. The observed XRD pattern is consistent with the selected area electron diffraction (SAED) pattern of the sample (Figure 1g). Both the XRD and SAED patterns suggest that the SPs are well multiple-crystallized. In addition, the peak of (111) is much higher than the other three crystal planes, indicating that the nanoarms on SPs are mainly oriented with (111), as demonstrated in Figure 1e.

Figure 1c,d presents the well-defined "meatball"-like SPs assembled with plentiful curved nanoarms. The arrows in Figure 1c show these nanoarms to possess hollow, soft, and tube-like nanomorphology. To elucidate the seed-mediated growth mechanism of the nanoarms and their self-assembly process into SPs, we studied the shape evolution of "meatball"-like SPs. To catch any possible short lifetime intermediates from the growth process of SPs, the growth process in a small-volume solution was quenched at differing times with a large amount of ice−water (Supporting Information). Interestingly, as shown in Figure 2, the complex units (immature SPs) with nanoarms assembled on individual cores appear in 1 min (Figure 2**a**), indicating that the nanoarms are formed quickly right after the addition of seeds to the growth solution. Over time, the SPs grow in size with more nanoarms assembled on cores (indicated by a yellow

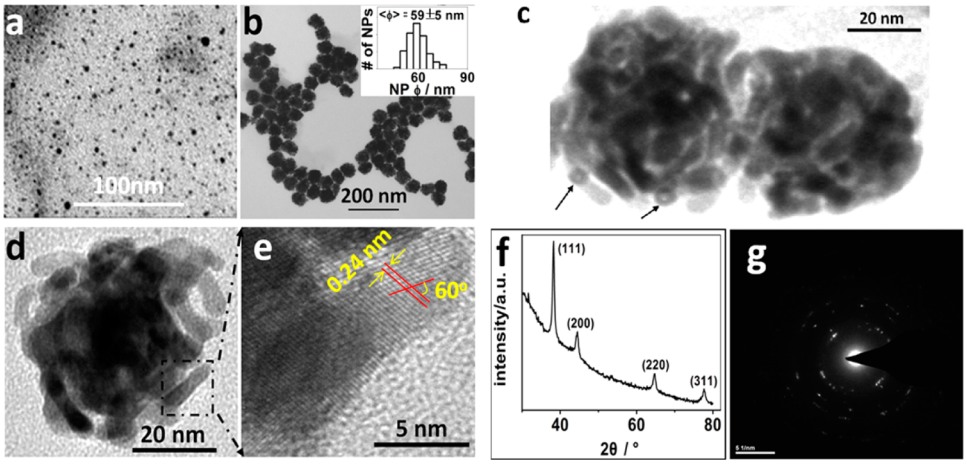

Figure 1. Characterization of gold nanoparticles. (a) TEM image of gold seeds with the average size of about 4 nm. (b) A typical TEM image of "meatball"-like SPs with average diameter of about 59 nm. (c) A high magnification TEM image of two SPs with arrows to indicate the hollow nanoarms on SPs. (d and e) High magnification TEM image of a SP and its corresponding high resolution TEM image on one nanoarm. (f) XRD pattern of gold SPs of the average diameter of 59 nm. (g) The correlated SAED pattern of Au SPs.

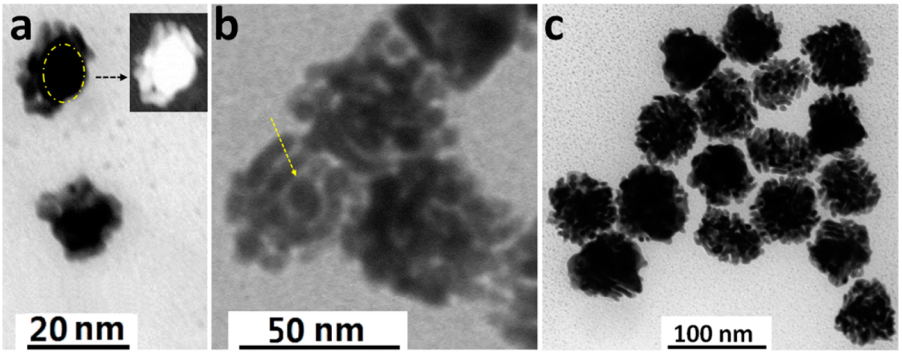

Figure 2. TEM images of the gold SPs sampled at different reaction times: (a) 1 min, (b) 5 min, (c) 10 min, respectively. The insert in (a) is the color-inverted image to show a core surrounded by a few nanoarms. The yellow arrow in (b) indicates the core in this SP.

arrow in Figure 2b). After about 10 min of the reaction, the color of the reaction solution becomes a stable dark blue, suggesting that the reaction is complete and mature core–shell morphology of SPs is obtained (Figure 2c). The cores of the mature SPs can no longer be observed from the TEM image on individual SPs, probably due to the thick multiple-layer assembly of nanoarms. The assembly process shown in Figure 2 is consistent with previous observations that nanoparticles with nonuniform size distributions can spontaneously assemble into uniformly sized SPs with core–shell morphologies where smaller nanoparticles pack in the outer shell and larger nanoparticles concentrate in the core.[2]

Figure 2 shows the growth process of SPs after nucleation of nanoarms on cores; however, it is still unclear how the nanoarms are formed and whether the nanoarm is really the first formation intermediate. Microfluidic experiments were conducted to bring clarity to this issue. It has been known that flow-based microfluidic systems can slow down the synthesis of nanowires and capture mechanistic details concerning their growth in solution phase.[26] Here, the flow-based microfluidic system is expected to slow down the formation and then the subsequent assembly process of the intermediate nanoarms due to a special microenvironment in constant flow.[26] On the basis of this technique, we expect to observe some new short-lifetime intermediates which are unresolvable from traditional synthesis process, and then deconvolute the detailed mechanism for the growth of SPs.

The flow-based microfluidic chip system is illustrated in Figure 3a and Supporting Information Figure S3. The three main reactants were flowed into the chip simultaneously through three independent syringes at the same flow rate. **Solution 1** was a solution of gold precursor $HAuCl_4$, **solution 2** contained gold seeds (as shown in Figure 1a), and **solution 3** was the reductant ascorbic acid solution. After the three components met at the microreactor, the seed-mediated growth of nanointermediates or SPs occurred spontaneously; the obtained product here, which probably contained some short lifetime intermediates for the growth of SPs, flowed rapidly through the outlet and was collected through a microtubing with different lengths (noted as **Tube1**, **Tube2**, **Tube3**, and **Tube4**, respectively) in ice–water, which quenched the SP growth immediately.[13] The different lengths of microtubing corresponded to different growth times of the intermediates (Figure 3a).

Figure 3b–e displays the typical TEM images of the obtained products with different growth times. From the shortest growth time (Figure 3b), the obtained intermediates from **Tube1** mostly comprise tiny, ultrathin and flexible gold nanoplates with an average thickness of about 2.5 nm (AFM image shown in Supporting Information Figure S4), thinner than any other Au nanoplates reported thus far.[27–29] With longer growth time (Figure 3c), the nanoplates obtained from **Tube2** become larger and many flexible cylinders or tubes are generated due to the folding or rolling up (Supporting Information Figure S5) of said flexible gold nanoplates as indicated by red and yellow arrows, respectively. The morphology of these rolled-up intermediates is congruous with the nanoarms on the "meatball"-like SPs obtained from traditional synthesis (Figure 1). This observation reveals that the ultrathin gold nanoplates, rather than the nanoarms, are the first type of intermediates in this synthesis. Therefore, nanoarm subunits observed on SPs shown in Figure 1 are actually a second-order nanostructure of ultrathin nanoplates. This semiopen morphology is distinct from a perfectly closed tube, such as the well-studied structure of carbon nanotubes (CNTs) (Supporting Information Figures S5–S6).[30,31]

With additional SP formation time observed in Figure 3d, we can see the initial stage of the seed-mediated SP growth in **Tube3**. The cores indicated by yellow arrows are indicative of rolled up Au nanoplates compacting together, also observed in HRTEM (Supporting Information Figure S7). Further, we can see the assembly of ultrathin Au nanoplates with complete or incomplete rolling up on the periphery of these cores. As the growth process goes further within even longer microtubing (Figure 3e,f), some immature

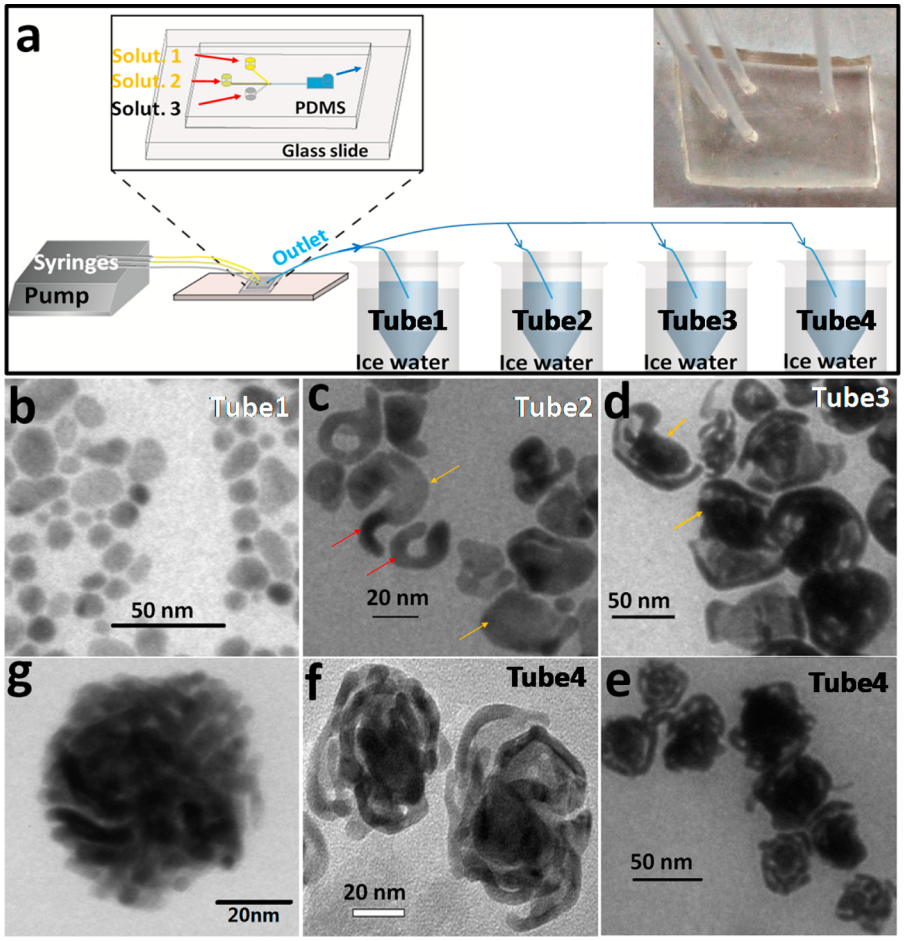

Figure 3. Flow-based microfluidic system and corresponding TEM results. (a) Scheme of the flow-based microfluidic system to capture the intermediates. Solutions 1, 2 and 3 are flowed in the microreactor from three independent syringes with the same flow rates controlled by a micropump. The product flowing out from the outlet is collected in ice−water through microtubing with different lengths noted as Tube1, Tube2, Tube3 and Tube4. The inset is the real image of the microfluidic chip. (b)Typical TEM image of the product from Tube1. (c) Typical TEM image of the product from Tube2. (d) Typical TEM image of the product from Tube3. (e and f) Typical TEM images of product from Tube4. (g) Typical TEM image of a mature Au SP obtained from microfluidic system with no ice−water quenching.

"meatball"-like SPs can be found in the obtained products from **Tube4**. If the products flowing out from the outlet are collected from **Tube4** without ice−water to quench the growth, then after 24 h, we are able to observe mature Au SPs as the final products shown in Figure 3g and compare against Figure 1. All collected data shown above unambiguously confirm the observed ultrathin gold nanoplates, rather than the hollow, soft nanoarms, to be the real first type of intermediate for the growth of Au SPs. These gold nanoplates have relatively high surface energy due to the large surface area; if the nanoplates are thin and flexible enough, they will decrease their surface energy by rolling into compact cylinders or tubes in solution spontaneously, forming the building-blocks for the growth of SPs. Thicker Au nanoplates cannot roll up and tend to stack up when dry (Supporting Information Figure S8).

From the above facts, we can therefore conclude that the interconnected nanoarms on SPs originate from the rolling of ultrathin gold nanoplates, as evidenced by the hollow structures or interspaces inside the individual entity as indicated by arrows in Figure 1c. In addition, the SP cores are also composed of compact nanoarms. We thus propose the following growth mechanism of "meatball"-like SPs in the traditional synthesis (Figure 4). When the seeds, gold precursors and the reductants are mixed in the solution, the seed-mediated growth of ultrathin soft gold nanoplates occurs immediately where each seed serves as a catalytic reaction center[32,33] to promote the reaction between gold precursor and ascorbic acid (a → b: ***step-i***).[27,28,34] The intermediate ultrathin nanoplates then roll up rapidly to form compact nanoarms in solution due to the high surface energy of these nanoplates (b → c: ***step-ii***). To further decrease the surface energy of the system or as a result of the van der Waals (vdW) attraction, these flexible soft nanoarms will self-assemble onto the surface of larger bundles of Au nanoarms nearest to them,[2] leading eventually to the growth of "meatball"-like SPs (c → d: ***step-iii***). Finally, more and more nanoarms will assemble on these units

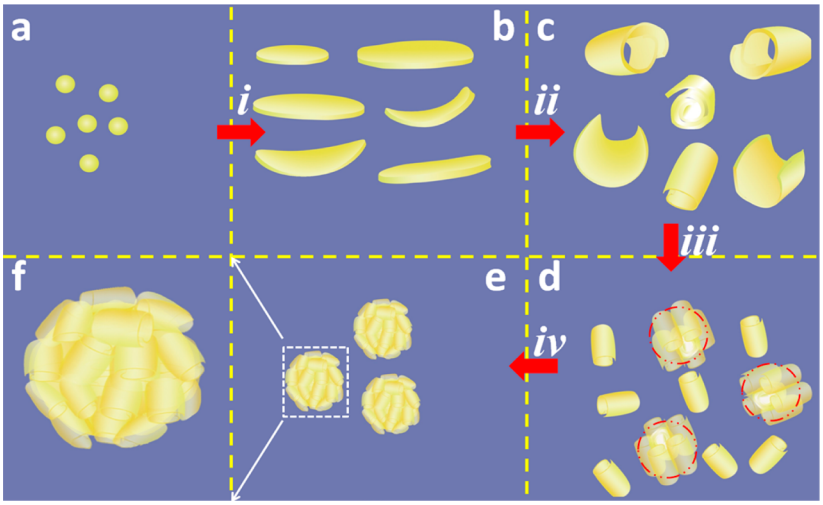

Figure 4. Scheme of the growth mechanism of gold SPs. (a → b: *step i*) Seed-mediated growth of the ultrathin gold nanoplates; (b → c: *step ii*) folding or rolling up of ultrathin gold nanoplates into flexible hollow nanoarms; (c → d: *step iii*) self-assembly of flexible hollow nanoarms of forming core/shell nanostructure to trigger the growth of SPs. The red circles indicate the cores for the following growth of SPs; (d → e: *step iv*) seed-mediated further growth of SPs by the random self-assembly of nanoarms on cores ; (f) magnification of a single "meatball"-like gold SP shown in e.

until a balance of electrostatic repulsion and vdW attraction is achieved, resulting in fully multiple-layered mature "meatball"-like SPs (d → e: ***step-iv*** and f).

The above deconvolution of SP growth mechanism highlights the significant role that the flow-based microfluidic chip plays. Without it, the ultrathin gold nanoplate intermediates, would not be observed, and it would be uncertain whether the only observable second-order structure, the rolled-up hollow nanoarms, were closed tubes like CNTs or not. In the deconvoluted growth mechanism of gold SPs, there are two seed-mediated growth steps. The first is the small gold seed (4 nm)-mediated growth of ultrathin gold nanoplates. The second one is the larger seed (compact gold nanoarms)-mediated growth of SPs triggered by the self-assembly of nanoarms.

To better understand the self-limiting growth of gold SPs, we applied Monte Carlo simulations to mimic the self-assembly process of flexible nanoarms (see Supporting Information, for details). In the simulation, the few, larger nanoarms are modeled as cylinders, whereas other nanoarms are reduced as rods. Clearly, the self-assembled structures are mainly dominated by interactions between the assembled building blocks, including van der Waals (vdW) attraction and the electrostatic repulsion between the nanoparticles.[2] Since the cylindrical nanoparticles are normally far away from each other as shown in TEM images, the vdW attraction between two cylindrical nanoparticles can be neglected. Therefore, only the vdW attraction between cylinders and rods, the vdW attraction between rods, the electrostatic repulsion between the rods, and the electrostatic repulsion between the cylinders and rods are considered in the simulation. A Lennard-Jones 12−6 potential was used for vdW attraction between nanoparticles, and a screened

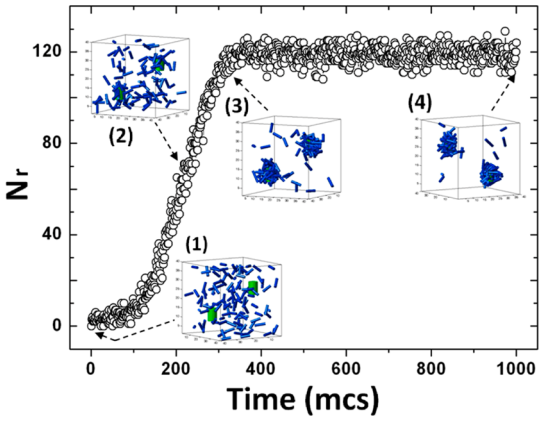

Figure 5. Variation of the number of the rods assembled onto the cyinder cores with Monte Carlo time. $\varepsilon_{CR} = 18$, $\varepsilon_{RR} = 7$, $A_{CR} = 2$, and $A_{RR} = 2$. The rods number is set as 140. (1) $t = 0$; (2) $t = 200$; (3) $t = 325$; (4) $t = 1000$. Green square represents the cylinder cores, while blue square represents the rods.

Coulomb potential was used for electrostatic interaction (Supporting Information). Figure 5 presents the variation of the number of rods assembled onto two cylindrical cores with Monte Carlo time (Monte Carlo step, *mcs*) at $\varepsilon_{CR} = 18$ (vdW attraction strength between cylinders and rods), $\varepsilon_{RR} = 7$ (vdW attraction strength between rods), $A_{CR} = 2$ (strength of the electrostatic repulsion between cylinders and rods), and $A_{RR} = 2$ (strength of the electrostatic repulsion between rods). A series of snapshots showing the formation of "meatball"-like nanoparticles at different times are also inserted in Figure 5. The number of assembled rods (N_r) shows a steady increase with time until $t = 325$ and then remains mostly unchanged as time is further increased. The inserted snapshots highlight that the cylinders and rods assemble into two almost monodisperse SPs at $t = 325$ (snapshots 1−3), and then these

two SPs mostly remain unchanged with time even though there are still some unassembled rods in the simulation box (snapshots 3−4), well reproducing the self-limiting growth observed in experiments. No significant changes can be found in the size of SPs even after increasing the number of rod in the simulation box, as shown in Supporting Information Figure S9, confirming the self-limiting behavior in size.

From the self-assembly of "meatball"-like nanoparticles, it is clear the vdW attraction (especially between rods) is the driving force of the continued growth of the SPs, whereas the electrostatic repulsion (especially between the rods) tends to disassemble the SPs. It has been proposed before that the self-limiting growth of SPs is governed by a balance between electrostatic repulsion and vdW attraction.[2] According to this theoretical analysis, an increase of the vdW attraction will lead to additional growth of SPs. Conversely, the SPs will become smaller or be disassembled when the electrostatic repulsion is increased. In Supporting Information Figure S10, we present a series of morphologies for SPs as a function of the vdW attraction strength between the rods (e_{RR}). As e_{RR} is increased, more and more free rods are assembled onto the SPs, indicating the continued growth of the SPs. On the other hand, it is observed that SPs start to become smaller and then disassemble as the strength of the electrostatic repulsion between the rods (A_{RR}) is increased, as shown in Supporting Information Figure S11.

Supporting Information Figure S12 demonstrates the shape-dependent optical property of Au SPs at different self-assembly stage, it is clear that the Au surface plasmon resonance (SPR) peak shifts positively from 590 nm (for ultrathin Au nanoplates shown in Figure 3b) to 630 nm (for mature Au SPs shown in Figure 1b) after the self-limiting growth of SPs. The red-shift observed here is consistent with previous observation of self-assembly of Au nanoparticles.[24]

Finally, the effect of surfactants on the seeded-growth of Au SPs is investigated.[35−38] It is well-known that halide ions tend to adsorb on low-index gold surfaces with binding energy that scales with polarizability $I^- > Br^- > Cl^-$ and surface energies with (111) > (110) > (100).[39] For the case here with cetyltrimethylammonium chloride (CTAC) as surfactant, the selective protection of Cl^- ions to the (111) facets of Au seeds leads to the preferential growth of Au nanoplates with the exposure of (111) facet (Figure 1). Compared with the Au nanoplates synthesized with cetyltrimethylammonium bromide (CTAB) as the surfactant,[40] due to the stronger binding ability of Br^- than Cl^- on Au (111) facet,[39] the protection of Cl^- to the (111) facet is insufficient and unstable. The insufficiency of Cl^--protection makes the apparent surface energy of (111) facets higher than that protected with Br^-. Therefore, the high surface energy of Au nanoplates protected with Cl^- can easily drive them to roll into nanoarms, and then self-assemble into spherical supraparticles.

CONCLUSIONS

In summary, a facile one-step strategy was introduced to synthesize the self-limiting spherical "meatball"-like Au SPs with two different building blocks. With a flow-based microfluidic chip, ultrathin gold nanoplates were found to be the first structural intermediates, which cannot be observed in traditional synthesis due to their rapid rolling-up to form the second-order nanostructure of flexible hollow nanoarms. The nucleation-based growth mechanism of SPs was then deconvoluted in detail based on solid evidence for two seed-mediated growth steps. The combination of traditional synthesis with flow-based microfluidic chips represent a new powerful tool to deconvolute complex growth or reaction mechanisms at nanometer scale by discovery of transient steps or short-lifetime intermediates which are usually neglected in traditional methods alone.

MATERIALS AND METHODS

Traditional Synthesis of Gold "Meatball"-like SPs. A growth solution was prepared in a centrifugal tube. First, 0.32 g of CTAC surfactant was added. Then, 9.625 mL of deionized water was placed into the tube to form a 0.10 M CTAC solution. The tube was then kept in a water bath set at 30 °C. Next, 250 μL of 0.01 M $HAuCl_4$ solution and 10 μL of 0.01 M NaBr solution were added to the tube. Finally, 90 μL of 0.04 M ascorbic acid was introduced. Then, 25 μL of the seed solution was added to the solution in the tube with gentle shaking until the solution color turned light blue (~20 s). The solution was left undisturbed for 10 min for particle growth and centrifuged at 12 000 rpm for at least 15 min to stop the reaction.

Microfluidic System To Investigate the Growth Process of SPs. The device design consists of a microchannel (400 μm × 400 μm cross-section and 3 cm long) with three inlets and one outlet. The three inlets have identical channel widths of 100 μm, and the angle between two adjacent inlet channels is 20°. The microfluidic device was fabricated using standard soft lithography with SU8-2100 master mold on a silicon substrate. SU-8-2100 photoresist (MicroChem Corp) was first spin-coated on a 4 in. silicon wafer at 500 rpm for 10 s followed by 2000 rpm for 30 s to obtain the desired thickness (400 μm). The coated wafer was soft-baked for 1 h at 95 °C and then exposed to ultraviolet light with exposure energy of 400 mJ/cm^2 through a photomask containing the pattern of microfluidic channels. After exposure, the wafer was baked again at 95 °C for 25 min and soaked in SU-8 developer (MicroChem Corp) to dissolve the unexposed photoresist. The patterned SU-8 master mold was then hard-baked at 150 °C for 15 min to anneal any microcracks in SU-8. PDMS (Sylgard 184, Dow Corning) molds were cast from the master, and inlets and outlets were created using a 16-gauge blunt-tipped needle. Molds were sealed to glass coverslips after treatment with oxygen plasma. Microbore tubing was seated directly into the inlet and outlet holes, providing a water-tight seal.

Conflict of Interest: The authors declare no competing financial interest.

Acknowledgment. Work was funded by the National Basic Research Program of China (973 Program, 2014CB932700,

2012CB932800 and 2012CB215500), National Natural Science Foundation of China (21273220, 21303180, 21422307, 51373172, 51433009) and "the Recruitment Program of Global youth Experts" of China.

Supporting Information Available: Experimental sections; characterizations; Monte Carlo simulations. This material is available free of charge *via* the Internet at http://pubs.acs.org.

REFERENCES AND NOTES

1. Zhuang, J. Q.; Wu, H. M.; Yang, Y. A.; Cao, Y. C. Supercrystalline Colloidal Particles from Artificial Atoms. *J. Am. Chem. Soc.* **2007**, *129*, 14166–14167.
2. Xia, Y. S.; Nguyen, T. D.; Yang, M.; Lee, B.; Santos, A.; Podsiadlo, P.; Tang, Z. Y.; Glotzer, S. C.; Kotov, N. A. Self-Assembly of Self-Limiting Monodisperse Supraparticles from Polydisperse Nanoparticles. *Nat. Nanotechnol.* **2011**, *6*, 580–587.
3. Lu, Z. D.; Yin, Y. D. Colloidal Nanoparticle Clusters: Functional Materials by Design. *Chem. Soc. Rev.* **2012**, *41*, 6874–6887.
4. Shevchenko, E. V.; Talapin, D. V.; Rogach, A. L.; Kornowski, A.; Haase, M.; Weller, H. Colloidal Synthesis and Self-Assembly of $CoPt_3$ Nanocrystals. *J. Am. Chem. Soc.* **2002**, *124*, 13958–13959.
5. Edwards, E. W.; Wang, D. Y.; Lhwald, H. M. Hierarchical Organization of Colloidal Particles: From Colloidal Crystallization to Supraparticle Chemistry. *Macromol. Chem. Phys.* **2007**, *208*, 439–445.
6. Yamada, Y.; Tsung, C. K.; Huang, W.; Huo, Z. Y.; Habas, S. E.; Soejima, T.; Aliaga, C. E.; Somorjai, G. A.; Yang, P. D. Nanocrystal Bilayer for Tandem Catalysis. *Nat. Chem.* **2011**, *3*, 372–376.
7. Lu, Z. D.; Ye, M. M.; Li, N.; Zhong, W. W.; Yin, Y. D. Self-Assembled TiO_2 Nanocrystal Clusters for Selective Enrichment of Intact Phosphorylated Proteins. *Angew. Chem., Int. Ed.* **2010**, *49*, 1862–1866.
8. Bai, F.; Wang, D. S.; Huo, Z. Y.; Chen, W.; Liu, L. P.; Liang, X.; Chen, C.; Wang, X.; Peng, Q.; Li, Y. D. A Versatile Bottom-up Assembly Approach to Colloidal Spheres from Nanocrystals. *Angew. Chem., Int. Ed.* **2007**, *46*, 6650–6653.
9. Klajn, R.; Bishop, K. J. M.; Fialkowski, M.; Paszewski, M.; Campbell, C. J.; Gray, T. P.; Grzybowski, B. A. Plastic and Moldable Metals by Self-Assembly of Sticky Nanoparticle Aggregates. *Science* **2007**, *316*, 261–264.
10. Lim, I. I. S.; Maye, M. M.; Luo, J.; Zhong, C. J. An Assessment of the Thermodynamic Driving Force for the Mediator-Template Assembly of Nanoparticles. *J. Phys. Chem. B* **2005**, *109*, 2578–2583.
11. Wang, T.; Zhuang, J.; Lynch, J.; Chen, O.; Wang, Z.; Wang, X.; LaMontagne, D.; Wu, H.; Wang, Z.; Cao, Y. C. Self-Assembled Colloidal Superparticles from Nanorods. *Science* **2012**, *338*, 358–363.
12. Ye, X.; Chen, J.; Engel, M.; Millan, J. A.; Li, W.; Qi, L.; Xing, G.; Collins, J. E.; Kagan, C. R.; Li, J.; *et al.* Competition of Shape and Interaction Patchiness for Self-Assembling Nanoplates. *Nat. Chem.* **2013**, *5*, 466–473.
13. Wu, H. L.; Kuo, C. H.; Huang, M. H. Seed-Mediated Synthesis of Gold Nanocrystals with Systematic Shape Evolution from Cubic to Trisoctahedral and Rhombic Dodecahedral Structures. *Langmuir* **2010**, *26*, 12307–12313.
14. Kim, F.; Conner, S.; Song, H.; Kuukendall, T.; Yang, P. D. Platonic Gold Nanocrystals. *Angew. Chem., Int. Ed.* **2004**, *43*, 3673.
15. Shankar, S. S.; Rai, A.; Ankamwar, B.; Singh, A.; Ahmad, A.; Sastry, M. Biological Synthesis of Triangular Gold Nanoprisms. *Nat. Mater.* **2004**, *3*, 482–488.
16. Su, Y. H.; Lai, W. H.; Chen, W. Y.; Hon, M. H.; Chang, S. H. Surface Plasmon Resonance of Gold Nano-Sea-Urchin. *Appl. Phys. Lett.* **2007**, *90*, 181905–181907.
17. Zhou, C.; Jiang, X.; Yang, L.; Yin, Y. D.; Jin, M. Low-Temperature Carbon Monoxide Oxidation with Au–Cu Meatball-Like Cages Prepared by Galvanic Replacement. *ChemSusChem* **2013**, *6*, 1883–1887.
18. Wang, H.; Halas, N. J. Mesoscopic Au "Meatball" Particles. *Adv. Mater.* **2008**, *20*, 820–825.
19. Wang, J.; Zhang, X.; Wang, Z.; Wang, L. M.; Xing, W.; Liu, X. One-Step and Rapid Synthesis of "Clean" and Monodisperse Dendritic Pt Nanoparticles and Their High Performance toward Methanol Oxidation and p-Nitrophenol Reduction. *Nanoscale* **2012**, *4*, 1549–1552.
20. You, H.; Ji, Y.; Wang, L.; Yang, S.; Yang, Z.; Fang, J.; Song, X.; Ding, B. Interface Synthesis of Gold Mesocrystals with Highly Roughened Surfaces for Surface-Enhanced Raman Spectroscopy. *J. Mater. Chem.* **2012**, *22*, 1998–2006.
21. Wang, L.; Wang, H.; Nemoto, Y.; Yamauchi, Y. Rapid and Efficient Synthesis of Platinum Nanodendrites with High Surface Area by Chemical Reduction with Formic Acid. *Chem. Mater.* **2010**, *22*, 2835–2841.
22. Zhong, L.; Zhai, X.; Zhu, X.; Yao, P.; Liu, M. Vesicle-Directed Generation of Gold Nanoflowers by Gemini Amphiphiles and the Spacer-Controlled Morphology and Optical Property. *Langmuir* **2010**, *26*, 5876–5881.
23. Fang, J.; Du, S.; Lebedkin, S.; Li, Z.; Kruk, R.; Kappes, M.; Hahn, H. Gold Mesostructures with Tailored Surface Topography and Their Self-Assembly Arrays for Surface-Enhanced Raman Spectroscopy. *Nano Lett.* **2010**, *10*, 5006–5013.
24. Maye, M. M.; Lim, I. I. S.; Luo, J.; Rab, Z.; Rabinovich, D.; Liu, T.; Zhong, C. J. Mediator-Template Assembly of Nanoparticles. *J. Am. Chem. Soc.* **2005**, *127*, 1519–1529.
25. Xia, Y. S.; Tang, Z. Y. Monodisperse Inorganic Supraparticles: Formation Mechanism, Properties and Applications. *Chem. Commun.* **2012**, *48*, 6320–6336.
26. Laocharoensuk, R.; Palaniappan, K.; Smith, N. A.; Dickerson, R. M.; Werder, D. J.; Baldwin, J. K.; Hollongsworth, J. A. Flow-Based Solution-Liquid-Solid Nanowire Synthesis. *Nat. Nanotechnol.* **2013**, *8*, 660–666.
27. DuChene, J.; Niu, W.; Abendroth, J. M.; Sun, Q.; Zhao, W.; Huo, F.; Wei, W. D. Halide Anions as Shape-Directing Agents for Obtaining High-Quality Anisortropic Gold Nanostructures. *Chem. Mater.* **2013**, *25*, 1392–1399.
28. Ah, C. S.; Yun, Y. J.; Park, H. J.; Kim, W. J.; Ha, D. H.; Yun, W. S. Size-Controlled Synthesis of Machinable Single Crystalline Gold Nanoplates. *Chem. Mater.* **2005**, *17*, 5558–5561.
29. Huang, X.; Li, H.; Li, S.; Wu, S.; Boey, F.; Ma, J.; Zhang, H. Synthesis of Gold Square-Like Plates from Ultrathin Gold Square Sheets: The Evolution of Structure Phase and Shape. *Angew. Chem., Int. Ed.* **2011**, *50*, 12245–12248.
30. Iijima, S.; Ichihashi, T. Single-Shell Carbon Nanotubes of 1-nm Diameter. *Nature* **1993**, *363*, 603–605.
31. Endo, M.; Iijima, S.; Dresselhaus, M. S. *Carbon Nanotubes*; Elsevier Science, Inc.: New York, 1996.
32. Sun, X. W.; Dong, S.; Wang, E. Large-Scale Synthesis of Micrometer-Scale Single-Crystalline Au Plates of Nanometer Thickness by a Wet-Chemical Route. *Angew. Chem., Int. Ed.* **2004**, *43*, 6360–6363.
33. Hu, J.; Odom, T. W.; Lieber, C. M. Chemistry and Physics in One Dimension: Synthesis and Properties of Nanowires and Nanotubes. *Acc. Chem. Res.* **1999**, *32*, 435–445.
34. Chu, H.-C.; Kuo, C.-H.; Huang, M. H. Thermal Aqueous Solution Approach for the Synthesis of Triangular and Hexagonal Gold Nanoplates with Three Different Size Ranges. *Inorg. Chem.* **2006**, *45*, 808–813.
35. Wang, W.; Han, Y.; Tian, M.; Fan, Y.; Tang, Y.; Gao, M.; Wang, Y. Cationic Gemini Surfactant-Assisted Synthesis of Hollow Au Nanostructures by Stepwise Reductions. *ACS Appl. Mater. Interfaces* **2013**, *5*, 5709–5716.
36. Fan, X.; Guo, Z. R.; Hong, J. M.; Zhang, Y.; Zhang, J. N.; Gu, N. Size-Controlled Growth of Colloidal Gold Nanoplates and Their High-Purity Acquisition. *Nanotechnology* **2010**, *21*, 105602–105607.
37. Wang, C.; Kan, C.; Zhu, J.; Zeng, X.; Wang, X.; Li, H.; Shi, D. Synthesis of High-Yield Gold Nanoplates: Fast Growth Assistant with Binary Surfactants. *J. Nanomater.* **2010**, *2010*, No. 969030.
38. Zhu, J.; Kan, C.; Li, H.; Cao, Y.; Ding, X.; Wan, J. Synthesis and Growth Mechanism of Gold Nanoplates with Novel Shapes. *J. Cryst. Growth* **2011**, *321*, 124–130.

39. Magnussen, O. M. Ordered Anion Adlayers on Metal Electrode Surfaces. *Chem. Rev.* **2002**, *102*, 679–725.
40. Millstone, J. E.; Hurst, S. J.; Métraux, G. S.; Cutler, J. I.; Mirkin, C. A. Colloidal Gold and Silver Triangular Nanoprisms. *Small* **2009**, *5*, 646–664.